Journal of Chemical&Engineering Data

pubs.acs.org/jced Article

Densities, Viscosities, and Self-Diffusion Coefficients of Aqueous Mixtures of $NaBH_4$, $NaB(OH)_4$, and NaOH Using the BH_4^- Delft Force Field (DFF/BH_4^-)

Julien R. T. Postma, Parsa Habibi, Poulumi Dey, Thijs J. H. Vlugt, Othonas A. Moultos, and Johan T. Padding*

Cite This: J. Chem. Eng. Data 2025, 70, 1830−1842

ABSTRACT: One of the most promising energy carriers for transport applications are hydrogen-based energy carriers. $NaBH_4$ is a hydrogen energy carrier and produces hydrogen bubbles when it is dissolved in water. The formation of hydrogen bubbles hinders experimental measurements of the thermodynamic and transport properties of aqueous $NaBH_4$ solutions at elevated temperatures. Accurate knowledge of these properties is essential for the $NaBH_4$ hydrolysis reactor modeling and design. Molecular dynamics (MD) simulations provide the option to study the thermodynamic and transport properties of $NaBH_4$ aqueous solutions without hindering hydrogen bubble formation. In this work, a new force field is developed for BH_4^-, namely, the Delft force field of BH_4^- (DFF/BH_4^-), which, combined with additional force fields, can accurately describe experimental densities and viscosities of 0 to 5 *m* (mol salt/kg water) $NaBH_4$, 0 to 3 *m* $NaB(OH)_4$, and 1 *m* NaOH aqueous solutions at 295 K within 1.8% and 10.8% maximum deviation, respectively. Empirical fitting correlations are created for densities, viscosities, and self-diffusivities obtained from the MD simulations of 0 to 5 *m* $NaBH_4$, 0 to 5 *m* $NaB(OH)_4$, and 0 to 1 *m* NaOH aqueous solutions at 295−363 K for $NaBH_4$ hydrolysis reactor modeling and design purposes.

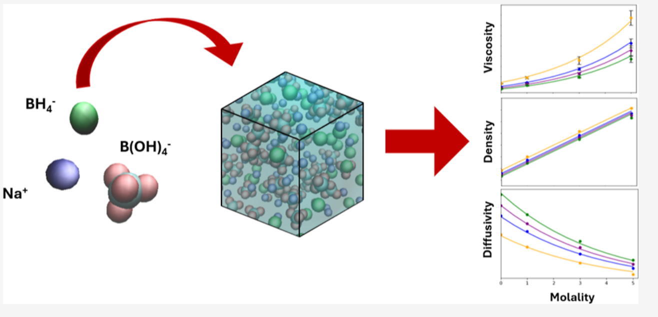

■ INTRODUCTION

Hydrogen-based energy carriers are investigated as one of the options to reduce greenhouse gas (GHG) emissions.[1−8] Hydrogen gas has a high gravimetric energy density of 120 to 142 MJ/kg and is therefore a prime candidate as an alternative energy carrier.[8−12] Unfortunately, the volumetric energy density of gaseous or liquefied hydrogen is limited, which is why there is an increased interest in alternatives that offer higher volumetric energy densities such as solid hydrogen carriers.[8,13−17] $NaBH_4$ is considered one of the most promising solid hydrogen carriers with a high gravimetric hydrogen capacity of 10.7 wt %.[8,18−23] $NaBH_4$ reacts with H_2O to create hydrogen gas and the side product $NaB(OH)_4$, following Reaction 1.[24−26] The reaction rate of Reaction 1 can be enhanced using a catalyst (based on Ru, Pt, Co, or Ni).[18,27−30]

$$NaBH_4(aq) + 4H_2O(l) \rightarrow NaB(OH)_4(aq) + 4H_2(g) \tag{1}$$

For $NaBH_4$, a potential use has been found in different transport applications (vehicles, small apparatuses, and drones) as a hydrogen-based energy carrier, due to its stable and safe storage in the solid state.[15,16,31−35] It should be noted that Reaction 1 is mainly considered for maritime applications[36] due to the continuous availability of water, utilizing reverse osmosis.[37,38] Reverse osmosis enables the conversion of brine to fresh water during the transport period, and hence, reducing the fuel weight requirement at the start of transport.[8,36,39,40]

As $NaBH_4$ reacts with water, an aqueous mixture of $NaBH_4$ and $NaB(OH)_4$ is formed.[27,29,41] Both the concentrations of $NaBH_4$ and $NaB(OH)_4$ change the thermodynamic and transport properties, such as density and viscosity, of aqueous solutions. Increasing the concentration of both $NaBH_4$ and $NaB(OH)_4$ by 5 *m* (mol salt/kg water) increases the viscosity by a factor of ca. 7, which influences the hydrodynamics of $NaBH_4$ hydrolysis reactors. To the best of our knowledge, limited information on thermodynamic and transport properties is available for aqueous solutions of $NaBH_4$ and mixtures of $NaBH_4$ with $NaB(OH)_4$, even though these properties are crucial for performance optimization of $NaBH_4$ hydrolysis reactors. The lack of available property data is most likely due to the difficulty of obtaining reliable experimental data, while $NaBH_4$ reacts in aqueous solution. The reaction of $NaBH_4$ in

Received: November 1, 2024
Revised: April 2, 2025
Accepted: April 4, 2025
Published: April 18, 2025

https://doi.org/10.1021/acs.jced.4c00629
J. Chem. Eng. Data 2025, 70, 1830−1842

aqueous solution forms hydrogen bubbles, which lead to inconsistencies in the experimental measurements of most thermodynamic and transport properties such as viscosity, density, and diffusivity.[19,24,25,42−44] Experimental measurements at higher temperatures (323−363 K) will only increase in difficulty due to the increase in the $NaBH_4$ hydrolysis reaction rate and H_2 bubble formation.[19,24,25,44] The $NaBH_4$ reaction and H_2 bubble formation can be reduced sufficiently with the addition of NaOH to the aqueous solution, according to Minkina et al.,[45] to measure thermodynamic and transport properties at lower temperatures (283−303 K) of $NaBH_4$ aqueous solutions.[46,47] Obtaining thermodynamic and transport properties at varying temperatures and salt compositions will provide further insight into the $NaBH_4$ hydrolysis reactor and $NaB(OH)_4$ crystallizer modeling and design.[48−54] The thermodynamic and transport properties of $NaBH_4$ and $NaB(OH)_4$ aqueous solutions without any bubbles have specific relevance in resolved multiphase computational fluid dynamics (CFD) simulations when the hydrogen bubbles and electrolyte solution are considered separately. Such resolved CFD simulations are urgently needed to understand and predict the interplay between hydrodynamics, mass and energy transfer, and reactions occurring in heterogeneously catalyzed systems. Furthermore, to predict the performance of a full $NaBH_4$ hydrolysis reactor system, it may be necessary to use effective mixture densities and viscosities of gas−liquid mixtures, which can also be found through resolved CFD simulations based on the results presented in this work.

Classical force field-based molecular dynamics (MD) simulations provide the solution to the bubble interference problem by not considering the chemical reaction of $NaBH_4$ with H_2O. For the MD simulations in this work, the Lennard-Jones (LJ) and electrostatic interactions are the only intermolecular interactions considered, while still providing accurate thermodynamic and transport properties of aqueous salt solutions compared with new experimental data at low temperatures (295 K).[55−58] A force field for BF_4^- was recently developed by Núñez-Rojas et al.[59] for $LiBF_4$ in propylene carbonate solutions, with a similar tetrahedral structure as BH_4^-. The fluorine atom of the BF_4^- force field has similar LJ parameters (σ = 4.47 Å and ϵ = 144.8 K) to the proposed LJ parameters of BH_4^-, which is most likely due to the similarities in size. A force field for $NaBH_4$ was already developed by Li,[60] but this force field describes interactions of BH_4^- and Na^+ with H_2O in the gaseous phase and the $NaBH_4$ (and $NaBH_4{\cdot}2H_2O$) crystal geometry, density, and compressibility in the solid state. Furthermore, the force field developed by Li[60] is not a LJ and partial charge force field and is therefore not considered comparable or compatible with the force field developed in this work. Hence, currently no force field is available for BH_4^- anions in aqueous solutions. In this work, a new classical force field is developed for $NaBH_4$ and compared with new experimental density and viscosity data at low temperatures and stabilized alkaline conditions. The force field is combined with the DFF/$B(OH)_4^-$ force field[56] and compared with new experimental density and viscosity data at low temperatures and stabilized alkaline conditions. Densities, viscosities, and self-diffusivities of $NaBH_4$ and $NaB(OH)_4$ aqueous solutions are computed at varying temperatures and salt compositions, based on expected hydrolysis reactor operating conditions (323−363 K and 1 bar). Empirical fitting correlations are created from the computed thermodynamic and transport properties of $NaBH_4$, $NaB(OH)_4$ and NaOH aqueous solutions, which can be used for modeling and design of $NaBH_4$ hydrolysis reactors.

EXPERIMENTAL METHOD

Solution Preparation. Experiments are performed to obtain thermodynamic and transport properties (density and viscosity) of stable $NaBH_4$ aqueous solutions at ambient conditions (295 K and 1 bar pressure). NaOH is added to experimental aqueous solutions of $NaBH_4$ [and $NaB(OH)_4$] to suppress the self-hydrolysis reaction of $NaBH_4$ (i.e., to prevent bubble formation) during the experimental measurements. All experimental aqueous solutions are stabilized with a 1 *m* NaOH (mol NaOH/kg water) concentration to obtain reliable and reproducible experimental data according to Minkina et al.[45] All solutions are prepared as follows. To stabilize the solution, NaOH is added to Milli-Q water first before adding $NaBH_4$. The experimental solutions of $NaBH_4$ and NaOH have a concentration range of 0 to 5 *m* $NaBH_4$ with 1 *m* NaOH. The experimental mixture solutions of $NaBH_4$, $NaB(OH)_4$, and NaOH are made in a similar way as the $NaBH_4$ solutions, but in a concentration range of 1 to 3 *m* $NaB(OH)_4$ with 1 *m* $NaBH_4$ and 1 *m* NaOH. The

Table 1. Details of All Species Used in the Experiments of This Work

component	chemical formula	CAS number	supplier	purity [%]
Milli-Q water	H_2O	7732-18-5		≥99.9
sodium hydroxide	NaOH	1310-73-2	Sigma-Aldrich	≥99.9
sodium metaborate tetrahydrate	$NaBO_2{\cdot}4H_2O$	10555-76-7	Thermo Fisher Scientific	≥98.5
sodium borohydride	$NaBH_4$	16940-66-2	CPH Chemicals	≥98.0

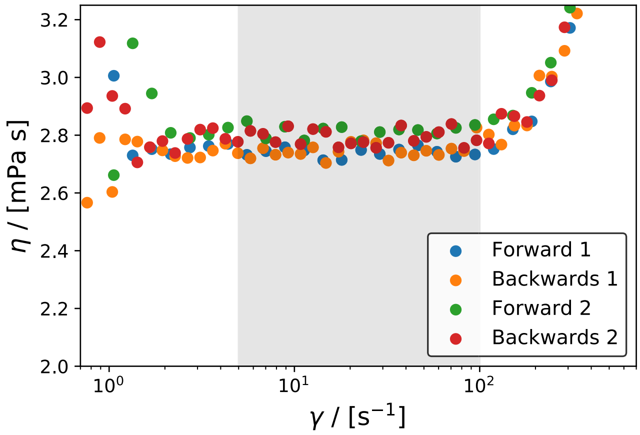

Figure 1. Viscosities (η) of $NaBH_4$, NaOH, and $NaB(OH)_4$ aqueous solutions vs shear rate (γ). The viscosity is measured using the MCR 320 rheometer with a 1 mm gap between the 50 mm diameter parallel plate and bottom plate to ensure low viscosity (close to 1 mPa s) stability. Four measurements are shown: two measurements with increasing shear rate as a function of time (i.e., Forward 1 and 2) and two measurements with decreasing shear rate (i.e., Backwards 1 and 2). The left part of the scatter curve shows low torque limits effects and the right part shows secondary flow effects. Both of these effects are common for plate rheometer measurements.[61] In between these limits, the gray area, a stable viscosity value can be measured (2.77 mPa s in this measurement).

https://doi.org/10.1021/acs.jced.4c00629
J. Chem. Eng. Data 2025, 70, 1830−1842

experimental mixture solutions of $NaBH_4$, NaOH, and $NaB(OH)_4$ are made using solid $NaBH_4$, solid $NaBO_2\cdot 4H_2O$, solid NaOH, and Milli-Q water. The $NaBO_2\cdot 4H_2O$ dissolves in water and forms $NaB(OH)_4$, as shown in Reaction 2. All materials used in the experiments can be found in Table 1. All experimental measurements are performed at a temperature of 295 K, and the composition of each solution is shown in Table 7.

$$NaBO_2\cdot 4H_2O(s) \rightarrow Na^+ + B(OH)_4^-(aq) + 2H_2O(l) \tag{2}$$

Density and Viscosity Experiments. The densities of the experimental solutions are measured using an Anton Paar density meter DMA 5000. The viscosity is measured using an Anton Paar Modular Compact Rheometer (MCR) 302. The rheometer uses a stainless steel parallel-plate geometry for the rotating top and a steady stainless steel bottom. The spacing between the plates is 1 mm and is entirely filled with the selected solution. The bottom and top are both heated to 295 K. After the desired temperature is reached, the top plate is rotated with a logarithmically increasing shear rate from 0.1 to 1000 s^{-1} (forward measurement), followed by a logarithmically decreasing shear rate from 1000 to 0.1 s^{-1} (backward measurement). All equipment used for the density and viscosity measurements is first calibrated with pure water and compared with literature values at a temperature of 295 K. Figure 1 shows a typical example of two separate forward (increasing shear rate) and backward (decreasing shear rate) viscosity measurements for a mixture of 1 *m* NaOH, 1 *m* $NaBH_4$, and 2 *m* $NaB(OH)_4$ aqueous solution. At low shear rates (ca. 0.1 to 5 s^{-1}), the measurements show fluctuating results due to low torque limit effects.[61] At medium shear rates (ca. 5 to 100 s^{-1}), the gray area, the fluctuations are reduced significantly and provide a stable measurement for the viscosity of the sample. At high shear rates (ca. 100 to 1000 s^{-1}), the apparent solution viscosity increases with shear rate due to secondary flow effects.[61] All viscosity measurements can be found in the Supporting Information Figure S1.

SIMULATION METHOD

Force Fields. H_2O is modeled using the four-site rigid TIP4P/2005[62] force field which accurately captures the density, diffusivity, and viscosity of pure H_2O for a wide range of conditions.[63−68] This force field is suitable not only for pure water, but also for salt solutions, such as NaCl,[57] NaOH,[55] and $NaB(OH)_4$[56] solutions, at varying concentrations, pressures and temperatures. Na^+ is described using the Madrid-2019[58] force field, which has a charge scaling of 0.85. Charge scaling was first proposed by Leontyev and Stuchebrukhov,[69−74] and it provides a simple way to correct for polarization effects in aqueous electrolyte solutions at the cost of less accurate predictions of properties such as free energies of hydration.[56,64−66] $B(OH)_4^-$ is modeled using the DFF/$B(OH)_4^-$[56] model with a charge scaling of 0.85. The DFF/$B(OH)_4^-$ model with a charge scaling of 0.85 *e* can accurately predict densities and viscosities of $NaB(OH)_4$ aqueous solution in the 0 to 5 *m* concentration range. OH^- is modeled using the Delft force field of OH^- (DFF/OH^-) model,[55] with a charge scaling of 0.85. The DFF/OH^- model yields accurate densities and viscosities values within the 0 to 3 *m* NaOH concentration range in aqueous solution.

The DFF/BH_4^- model is developed in this work, and the optimized LJ interaction parameters and charges can be found in Table 2. The DFF/BH_4^- model has a single interaction site, similar to the TraPPE CH_4 force field.[75] Due to the low atomic mass of hydrogen compared to boron, the lack of hydrogen bond interactions with the hydrogen atom, and the decrease in computational demand, a single interaction site is considered sufficient for the simulation of BH_4^-. The DFF/BH_4^- model is optimized using experimental densities and viscosities for varying concentrations of $NaBH_4$ at 295 K and 1 *m* NaOH aqueous solutions. All force field parameters [TIP4P/2005[62] water force field, Madrid-2019[58] Na^+ force field, DFF/OH^- force field,[55] DFF/$B(OH)_4^-$ force field[56] and the BH_4^- force field developed in this work] used in this study are shown in Tables S1−S5 of the Supporting Information and the CAS-numbers can be found in Table 3.

All molecules and ions are considered rigid and follow the Lorentz−Berthelot mixing rules except for the $Na^+/-O_w$ and $B(OH)_4^-/-O_w$ LJ interaction which are specified in Tables S2 and S5 of the Supporting Information.[76,77]

Simulation Settings. All MD simulations in this work are performed with the open-source large-scale atomic/molecular massively parallel simulator (LAMMPS)[78] (version August 2018). Interactions between any pair of ions or (nonbonded) atoms are described by an LJ (12-6) term and an electrostatic term. The SHAKE[79] and Rigid Body[80] algorithms in

Table 2. Force Field Parameters for BH_4^-[a]

force field	$q_{BH_4^-}$ [*e*]	$\epsilon_{BH_4^-}/k_B$ [K]	$\sigma_{BH_4^-}$ [Å]
DFF/BH_4^-	0.85	148	4.50

[a]The BH_4^- ion is modeled as a single interaction site in which all the hydrogen atoms are positioned inside the boron atom. BH_4^- has a total charge of 0.85 ($q_{BH_4^-}$), which is based on the charge scaling of Madrid-2019[58] (0.85). The LJ energy parameter $\epsilon_{BH_4^-}$ is based on the LJ energy parameter of CH_4 by Martin and Siepmann.[75] The values of ϵ and σ for all combinations with BH_4^- follow the Lorentz−Berthelot mixing rules.[76,77]

Table 3. Details of All Species Used in the MD Simulations of This Work

component	chemical formula	CAS number	force field
water	H_2O	7732-18-5	TIP4P/2005[62]
sodium	Na^+	7440-23-5	Madrid-2019[58]
hydroxide	OH^-	14280-30-9	DFF/OH^- force field[55]
tetrahydroxyborate	$B(OH)_4^-$	15390-83-7	DFF/$B(OH)_4^-$ force field[56]
borohydride	BH_4^-	16971-29-2	DFF/BH_4^- force field

Table 4. Number of Water, Na^+, BH_4^-, and OH^- Molecules Used in the MD Simulations for Mixture Type 1[a]

m_{NaBH_4}	m_{NaOH}	N_{H_2O}	N_{Na^+}	$N_{BH_4^-}$	N_{OH^-}	$\langle V\rangle$
1	1	1000	36	18	18	30,790
3	1	1000	72	54	18	32,972
5	1	1000	108	90	18	35,187

[a]m_x is in mol of ion *x*/kg water and *V* is the average volume of the simulation in units of Å^3. All simulations are run at 1 bar and 295 K and are used for optimization of the force field to minimize deviation from the experimental densities and viscosities at different concentrations of $NaBH_4$ and 1 *m* NaOH.

https://doi.org/10.1021/acs.jced.4c00629
J. Chem. Eng. Data 2025, 70, 1830−1842

Table 5. Number of Water, Na^+, $B(OH)_4^-$, BH_4^-, and OH^- Molecules Used in the MD Simulations for Mixture Type 2[a]

m_{NaBH_4}	$m_{NaB(OH)_4}$	m_{NaOH}	N_{H_2O}	N_{Na^+}	$N_{BH_4^-}$	$N_{B(OH)_4^-}$	N_{OH^-}	$\langle V \rangle$
1	1	1	1000	54	18	18	18	31,761
1	2	1	1000	72	18	36	18	32,681
1	3	1	1000	90	18	54	18	33,633

[a] m_x is in mol of ion x/kg water and V is the average volume of the simulation in units of Å^3. All simulations are run at 1 bar and 295 K and are used for optimization of the force field to minimize deviation from the experimental densities and viscosities at different concentrations of $NaB(OH)_4$ with 1 m $NaBH_4$ and 1 m NaOH.

Table 6. Number of Water, Na^+, $B(OH)_4^-$, BH_4^-, and OH^- Molecules Used in the MD Simulations for Mixture Type 3[a]

m_{NaBH_4}	$m_{NaB(OH)_4}$	N_{H_2O}	N_{Na^+}	$N_{BH_4^-}$	$N_{B(OH)_4^-}$	$\langle V \rangle$
1	0	1000	18	18	0	31,371
1	1	1000	36	18	18	32,383
1	3	1000	72	18	54	34,394
1	5	1000	108	18	90	36,423
3	0	1000	54	54	0	33,603
3	1	1000	72	54	18	34,609
3	3	1000	108	54	54	36,621
3	5	1000	144	54	90	38,633
5	0	1000	90	90	0	35,858
5	1	1000	108	90	18	36,869
5	3	1000	144	90	54	38,864
5	5	1000	180	90	90	40,857

[a] m_x is in mol of ion x/kg water and V is the average volume of the simulation in units of Å^3. All simulations are run at 1 bar and 323–363 K and are used as input data for empirical correlations at different concentrations of $NaB(OH)_4$ and $NaBH_4$.

LAMMPS[78] are used to fix the bond lengths and bond angles of all molecules and ions in the MD simulations. The Rigid Body[80] algorithm is used to accommodate the addition of $B(OH)_4^-$ ions and requires longer computation time. Therefore, only simulations which include $B(OH)_4^-$ ions use the Rigid Body[80] algorithm. All other simulations use the SHAKE algorithm.[79] The particle–particle particle–mesh (PPPM)[76,81−83] method is used to handle long-range electrostatic interactions (relative uncertainty of 10^{-5}). A cutoff radius of 10 Å is applied to the LJ and real space contribution of the electrostatic interactions. Analytic tail-corrections are applied for computing energies and pressures in the LJ interactions beyond a cutoff radius of 10 Å. To integrate the equation of motion, the Verlet algorithm[84] is used with a time step of 1 fs. Periodic boundary conditions are imposed in all directions. To maintain constant pressure and temperature, the Nosé–Hoover thermostat and barostat[76,85,86] are applied to all simulations with coupling constants of 100 and 1000 fs, respectively. The Nosé–Hoover algorithm is adjusted for rigid bodies, as proposed by Kamberaj.[87] The On-the-Fly Calculation of Transport Properties (OCTP)[88] plugin is used for computing the dynamic viscosities, densities, and self-diffusion coefficients of all species [H_2O, Na^+, $B(OH)_4^-$, BH_4^-, OH^-]. The initial configurations for each mixture type are created using PACKMOL[89] (v20.3.1). For each starting condition, the volume of the simulation box is determined by a 1 to 2 ns equilibration run in the isorbaric-isothermal (*NPT*) ensemble, followed by a 1 to 2 ns production run (*NPT* ensemble) to obtain the average box size. This average box size is subsequently used in the canonical (*NVT*) ensemble to compute the properties mentioned before. The *NVT* ensemble includes a 1 ns equilibration run (*NVT* ensemble) and a 10 to 30 ns production run (*NVT* ensemble). Densities are calculated using the average box volume from the *NPT* simulations. OCTP uses the Einstein relations[77,90−92] to compute the dynamic viscosities (shown in eq 3), which are not influenced by finite-size effects.[93−96]

$$\eta_{\alpha\beta} = \lim_{t\to\infty} \frac{1}{2t}\frac{V}{k_B T}\langle\left(\int_0^t P_{\alpha\beta}(t')\,dt'\right)^2\rangle \tag{3}$$

where η is the viscosity, t is time, k_B is Boltzmann's constant, T is temperature, and P represents the pressure tensor. Self-diffusivities for each ion/molecule are determined from the mean square displacements (MSD) (shown in eq 4).[77,97−101]

$$D_{i,\mathrm{self}}^{\mathrm{MD}} = \lim_{t\to\infty} \frac{1}{6N_i t}\langle\sum_{j=1}^{N_i}(r_{j,i}(t) - r_{j,i}(0))^2\rangle \tag{4}$$

where $D_{i,\mathrm{self}}$ is the self-diffusion coefficient for molecule/ion type i, N_i is the number of molecules/ions of type i, and $r_{j,i}$ represents the (unfolded) position of the j-th molecule/ion of species i. Equations 3 and 4 are valid at time scales where the slope of the MSD as a function of time is 1 in a log–log plot. The self-diffusivities are corrected for finite size effects using the Yeh–Hummer[94,102−104] correction, as shown in eq 5

$$D_{i,\mathrm{self}} = D_{i,\mathrm{self}}^{\mathrm{MD}} + \frac{k_B T \xi}{6\pi\eta L} \tag{5}$$

where η is the dynamic viscosity, which is not influenced by finite-size effects,[93−96] L is the length of the (cubic) simulation box, and ξ is a dimensionless number equal to 2.837298 for a cubic simulation box. The DelftBlue supercomputer[105] is used for performing MD simulations.

Mixture Types. MD simulations are performed for the following three mixture types. Mixture type 1 consists of 1000 H_2O molecules with 18 to 108 Na^+, 0 to 90 BH_4^-, and 18 OH^- ions at 295 K and 1 bar, as shown in Table 4. The average box size $\langle V \rangle$ in units of Å^3 is shown in Table 4 for each molality at 295 K and 1 bar. The MD simulations of mixture type 1 provide a comparable molality concentration range as applied in the $NaBH_4$ and NaOH aqueous solution experiments performed in this work.

Mixture type 2 consists of 1000 H_2O molecules with 54 to 90 Na^+, 18 to 54 $B(OH)_4^-$, 18 BH_4^-, and 18 OH^- ions at 295 K and 1 bar, as shown in Table 5. The average box size $\langle V \rangle$ in units of Å^3 is shown in Table 5 for each molality at 295 K and 1 bar. The MD simulations of mixture type 2 provide a comparable molality concentration range as applied in the $NaBH_4$, $NaB(OH)_4$, and NaOH aqueous solution experiments performed in this work.

Mixture type 3 consists of 1000 H_2O molecules with 18 to 180 Na^+, 0 to 90 $B(OH)_4^-$, and 18 to 90 BH_4^- at 323, 343, 353, and 363 K and 1 bar, as shown in Table 6. The average box size $\langle V \rangle$ in units of Å^3 is shown in Table 6 for each molality at

https://doi.org/10.1021/acs.jced.4c00629
J. Chem. Eng. Data 2025, 70, 1830−1842

323 K and 1 bar. The MD simulations of mixture type 3 provide a comparable molality concentration and temperature range as found in the operating conditions of $NaBH_4$ hydrolysis reactors.[50,51,106]

RESULTS AND DISCUSSION

BH_4^- Force Field (DFF/BH_4^-) Optimization. To obtain densities, viscosities, and self-diffusivities for $NaBH_4$ aqueous solutions from MD simulations, a force field for BH_4^- is required. For the MD simulations in this work, the LJ and electrostatic interactions are the only intermolecular interactions considered. For the MD simulations in this work, intramolecular interactions are not accounted for and a rigid structure is used. For both LJ and electrostatic interactions combined, three parameters can be used to optimize and tune the BH_4^- force field: σ (in units of Å), ϵ/k_B (in units of K), and q (in units of e). In this work, both q and ϵ/k_B are fixed to 0.85 e and 148 K, respectively. It should be noted that $q = 1$ is not considered in this work. In previous work, Joung−Cheatham developed a $q = 1$ nonpolarizable force field for NaCl, which was unsuccessful in simultaneously predicting both free energies of hydration and transport properties at higher molalities of NaCl.[107] Hence, to avoid this issue and maintain consistency in the Na^+ charge scaling in aqueous mixtures of

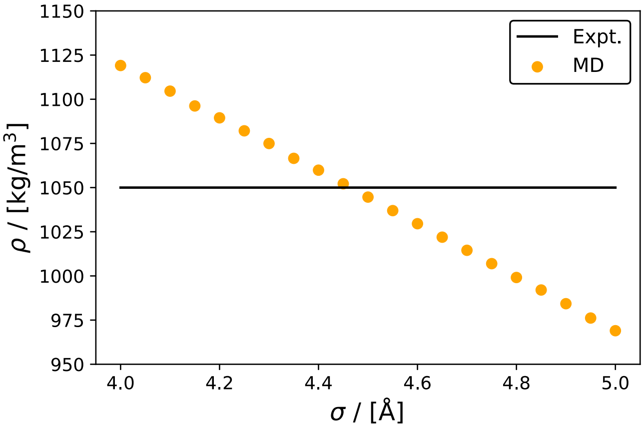

Figure 2. BH_4^- force field is optimized to match experimental density (ρ) measurements with the corresponding $\sigma_{BH_4^-}$ at 295 K and 1 bar. For the BH_4^- force field optimization, $\epsilon_{BH_4^-}/k_B$ and $q_{BH_4^-}$ are 148 K and 0.85 e, respectively. Both simulations and experiments use a 5 m concentration of $NaBH_4$ with 1 m NaOH in aqueous solution. The DFF/BH_4^- force field is combined with TIP4P/2005[62] water, Madrid-2019[58] Na^+ and DFF/OH^- force field.[55] An acceptable deviation (within 1.5%) from the experimental density is found for $\sigma_{BH_4^-}$ between 4.45, 4.50, and 4.55 Å. The error bars for densities are smaller than the symbol size and have therefore been removed for clarity. The densities and density uncertainties of the MD simulations for each sigma can be found in Table S8.

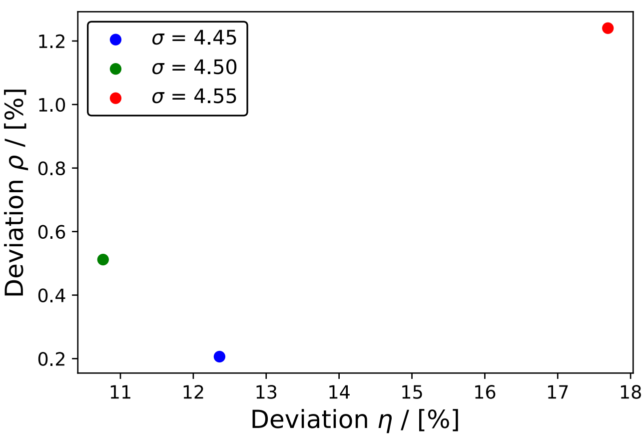

Figure 3. Deviations in density (ρ/[%]) vs deviations in viscosity (η/[%]) for experimental density and viscosity of 5 m [mol salt/kg water] $NaBH_4$ and 1 m NaOH in aqueous solution, compared to computed MD simulations of 5 m [mol salt/kg water] $NaBH_4$ and 1 m NaOH in aqueous solution at σ = 4.45 Å (blue), 4.50 Å (green), and 4.55 Å (purple). Force field parameters DFF/BH_4^- are used for the simulations, combined with TIP4P/2005[62] water, Madrid-2019[58] Na^+ and DFF/OH^- force field.[55]

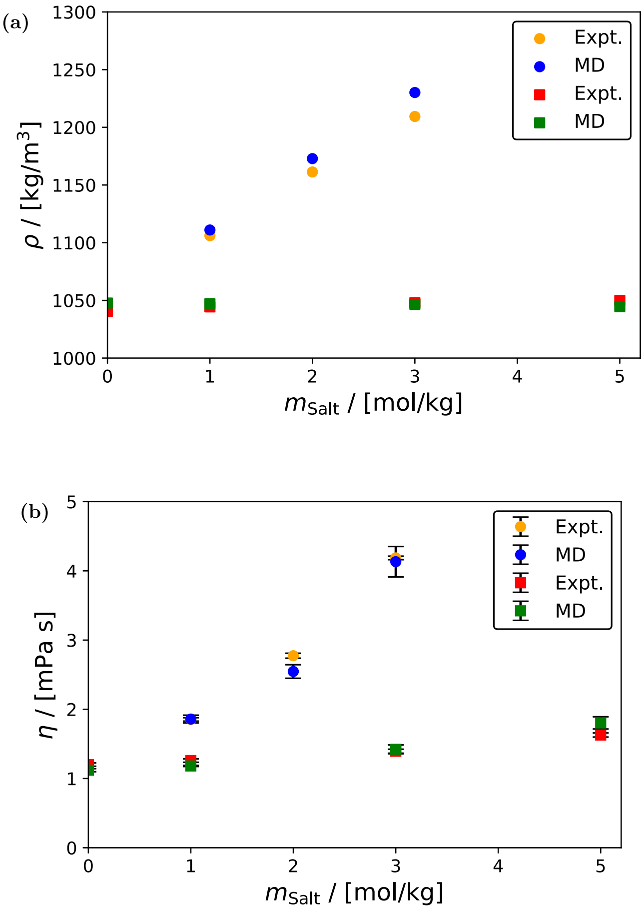

Figure 4. (a) Densities (ρ) and (b) viscosities (η) as a function of salt m [mol salt/kg water]. The square symbols (red: experiments, green: MD simulations) represent the densities and viscosities at different concentrations of $NaBH_4$ from 0 to 5 m [mol $NaBH_4$/kg water] with 1 m NaOH in aqueous solution at 295 K and 1 bar. The circle symbols (yellow: experiments, blue: MD simulations) represent the densities and viscosities at different concentrations of $NaB(OH)_4$ from 1 to 3 m [mol $NaB(OH)_4$/kg water] with 1 m $NaBH_4$ and 1 m NaOH in aqueous solution at 295 K and 1 bar. Force field parameters of DFF/BH_4^- are used for the simulations, combined with the TIP4P/2005[62] water, Madrid-2019[58] Na^+, DFF/$B(OH)_4^-$[56] and DFF/OH^- force field.[55] The error bars of viscosities for the experiments and MD simulations are presented as one standard deviation. The error bars for densities are smaller than the symbol size and have therefore been removed for clarity. The uncertainties of viscosity and density for experiments can be found in Table 7. Uncertainties for the MD simulations can be found in the Supporting Information Excel file provided.

https://doi.org/10.1021/acs.jced.4c00629
J. Chem. Eng. Data 2025, 70, 1830−1842

Table 7. Experimental Measurements of Density (ρ), One Standard Deviation of the Density Data (ρ_{error}), Viscosity (η), and One Standard Deviation of the Viscosity Data (η_{error}) for Different Concentrations of $NaBH_4$ and $NaB(OH)_4$ for Aqueous Solution of 1 *m* of NaOH Solutions at 295 K and 1 bar Pressure[a]

molality $NaB(OH)_4$ [*m* [mol salt/kg water]]	molality $NaBH_4$ [*m* [mol salt/kg water]]	ρ [kg/m^3]	ρ_{error} [kg/m^3]	η [mPa s]	η_{error} [mPa s]
0	0	1040.5	0.078	1.20	0.024
0	1	1044.4	0.43	1.26	0.025
0	3	1048.1	0.50	1.39	0.029
0	5	1050.0	0.21	1.63	0.030
1	1	1106.1	0.097	1.85	0.025
2	1	1161.2	0.10	2.82	0.036
3	1	1209.4	0.14	4.19	0.025

[a]Densities are measured using a DMA 5000 densitometer, and viscosity is measured with the MCR 320 rheometer. All solutions for these measurements are stabilized using 1 *m* of NaOH to prevent any hydrogen bubble formation during the measurements. The uncertainty of density (ρ_{error}) and viscosity (η_{error}) shown in this table are one standard deviation from the experimental data.

Na^+, BH_4^-, OH^-, and $B(OH)_4^-$, the value of q is fixed at 0.85. The value of ϵ/k_B is fixed at 148 K to match the energy minimum of methane (CH_4), which has a similar structure and size to BH_4^-.[75] Therefore, the force field is exclusively optimized using σ to minimize the deviation from experimental densities and viscosities within the desired concentration range of $NaBH_4$ (0 to 5 *m* $NaBH_4$ in aqueous solution). It should be noted that ion pairing, salt clustering, and crystallization do not occur in any of our MD simulations, as shown by the radial distribution functions (RDFs) in Figure S4 of the Supporting Information, as the anions are only present outside the second hydration layer of Na^+. If one would exclusively focus on the predicted density of a 5 *m* $NaBH_4$ with 1 *m* NaOH aqueous solution at 295 K, as used in the experiments, Figure 2 shows that the computed density has minimal deviation from the experimental density when σ is in the range of 4.45−4.55 Å (within 1.5% maximum deviation). The precise value of σ is chosen as a balance between matching the experimental density and matching the experimental viscosity of an aqueous solution of 5 *m* $NaBH_4$ with 1 *m* NaOH. Figure 3 shows that for all choices of σ within the range 4.45−4.55 Å, where the density deviation is acceptably small, the smallest viscosity deviation occurs at $\sigma = 4.50$. For the BH_4^- force field, therefore, a σ of 4.50 Å is chosen due to having the best agreement with viscosity, while maintaining a density deviation below 1%. The BH_4^- force field with a σ of 4.50 Å will be referred to as the DFF/BH_4^- and is used for the MD simulations. Figure 4a,b shows the experimental densities and viscosities (red squares) compared with MD simulations (green squares) for aqueous solutions of 0 to 5 *m* $NaBH_4$ with 1 *m* NaOH. The DFF/BH has maximum deviations for densities and viscosities of 0.7% and 10.8%, respectively, and average deviations of 0.4% and 6.4%, respectively, at 295 K compared with experimental data. The maximum deviation is defined as the largest deviation between a MD simulation compared with an experimental data point with a matching concentration, as shown in eq 6.

$$\sigma_{max} = \max_i\left(\left|1 - \frac{n_{k,i}}{n_{l,i}}\right|\right) \tag{6}$$

where $n_{k,i}$ is the ith data point for data type k (MD simulations or empirical fit inputs) and $n_{l,i}$ is the ith data point for data type l (experiments or MD simulations). The absolute average deviation is defined as the average of all deviations for each MD simulation compared with their respected experimental data point, as shown in eq 7

$$\sigma_{AA} = \frac{1}{N}\sum_{i=1}^{N}\left|1 - \frac{n_{k,i}}{n_{l,i}}\right| \tag{7}$$

where N is the size of the data set.

The self-diffusivity of BH_4^- is compared with a single experiment by Wang et al.[108] for which the diffusion coefficient of $(1.62 \pm 0.05) \times 10^{-9}$ m^2/s is measured with a concentration of 0.02 *m* $NaBH_4$ and 1 *m* NaOH at 303 K. A comparable BH_4^- self-diffusion coefficient of $(1.82 \pm 0.16) \times 10^{-9}$ m^2/s is found for simulations with a concentration of 0.11 *m* $NaBH_4$ and 1 *m* NaOH at 303 K after Yeh−Hummer correction. A concentration of 0.11 *m* of $NaBH_4$ is similar to adding two ions of BH_4^- to a system of 1000 water molecules; hence, using fewer ions would not provide reliable results. It should be noted that the corrected self-diffusion is in agreement with the experiment of Wang et al.[108] at infinite dilutions conditions despite the force field not being optimized on the self-diffusion of BH_4^-.

Experimental Salt Mixtures Compared with MD. In the previous subsection, the DFF/BH_4^- model was optimized using experimental aqueous solutions of $NaBH_4$ and NaOH. To use the DFF/BH_4^- model for hydrolysis reaction conditions, the research is extended to aqueous solutions of $NaBH_4$, $NaB(OH)_4$, and NaOH. Several mixture compositions are prepared for a comparative study between experiments and MD simulations. The experimental densities and viscosities measured for aqueous mixtures of 0 to 3 *m* $NaB(OH)_4$, 1 *m* $NaBH_4$, and 1 *m* NaOH at 295 K and 1 bar, respectively, are shown in Table 7. Figure 4a,b shows the experimental densities and viscosities (yellow circles) compared with MD simulation (blue circles) for aqueous mixture solutions of 1 to 3 *m* $NaB(OH)_4$, 1 *m* $NaBH_4$, and 1 *m* NaOH. The experimentally measured mixture densities and viscosities (yellow) match the mixture MD simulations (blue) within 1.8% maximum deviation for density and 8.3% maximum deviation for viscosity. It should be noted that the maximum deviations for densities only increased from 0.7 to 1.8%, and for viscosities, the maximum deviation decreased from 10.8 to 8.3% when extending the force field capabilities to experimental mixture solutions, while none of the force fields are further tuned for mixture solutions. The increase in maximum deviation from 0.7% to 1.8% in density for the DFF/BH_4^- is most likely caused by the accumulative deviations of all the additional force fields used in the mixture simulations. The maximum deviations of density and viscosity (1.8% and 10.8%) are similar to maximum deviations of densities and viscosities reported in other works (typically 0.5−2% and 5−

https://doi.org/10.1021/acs.jced.4c00629
J. Chem. Eng. Data 2025, 70, 1830−1842

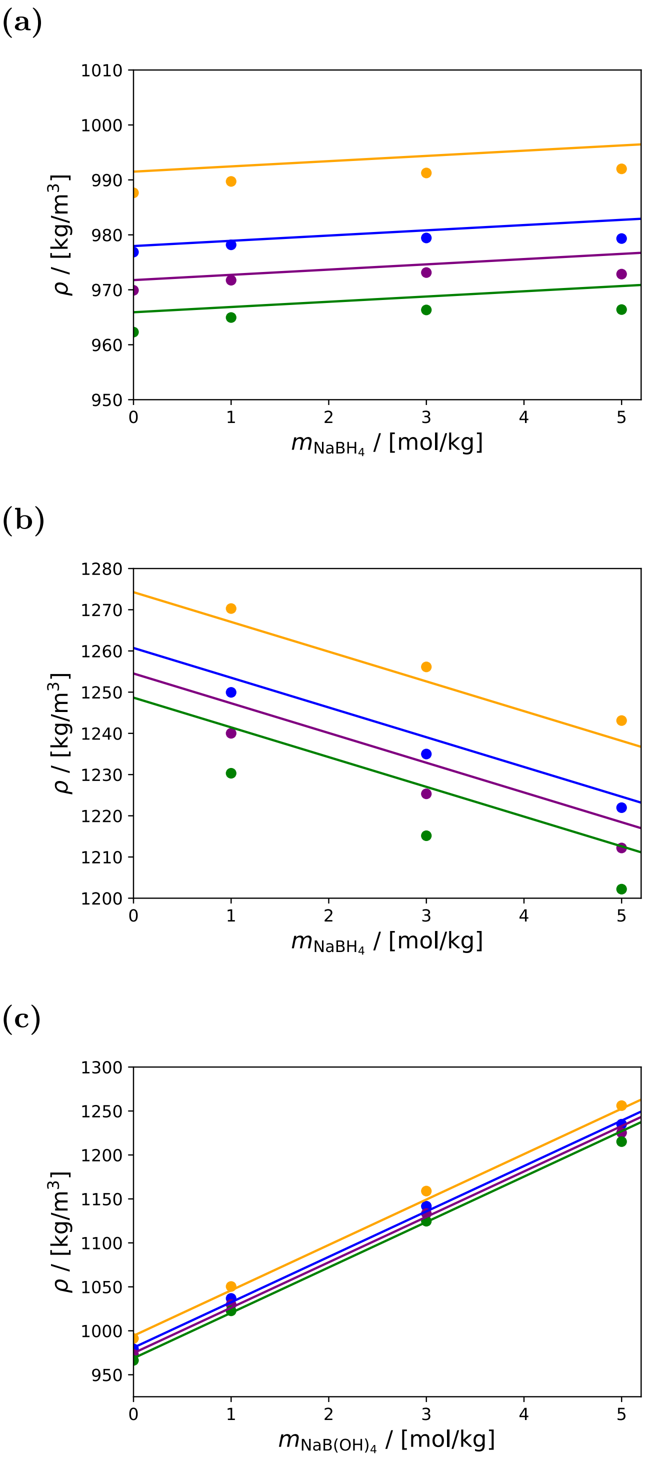

Figure 5. Computed densities (ρ) of $NaBH_4$ and $NaB(OH)_4$ aqueous solutions at 1 bar and 323 (yellow), 343 (blue), 353 (purple), and 363 (green) K are shown as circles in (a–c). (a) Densities for pure $NaBH_4$ aqueous solutions with the increasing $NaBH_4$ concentration at different temperatures. (b) Densities for $NaBH_4$ and $NaB(OH)_4$ aqueous solutions with a fixed $NaB(OH)_4$ concentration of 5 m and increasing $NaBH_4$ concentration at different temperatures. (c) Densities for $NaBH_4$ and $NaB(OH)_4$ aqueous solutions with a fixed $NaBH_4$ concentration of 3 m and increasing $NaB(OH)_4$ concentration at different temperatures. The empirical correlation is represented by solid lines and follows eq 8 with the parameters in Table 8. The error bars for densities are smaller than the symbol size and have therefore been removed for clarity. Uncertainties can be found in the Supporting Information Excel file provided.

Table 8. Density (ρ) Fitting Parameters of Eq 8 for $NaBH_4$, $NaB(OH)_4$, and NaOH Aqueous Solutions[a]

dependency	parameter	value	
n.a.	ρ_0	7.59×10^2	kg/m^3
$NaB(OH)_4$	A_1	5.66×10^1	kg/m^3 m_1^{-1}
$NaBH_4$	A_2	9.54×10^{-1}	kg/m^3 m_2^{-1}
NaOH	A_3	4.24×10^1	kg/m^3 m_3^{-1}
$NaB(OH)_4 \cdot NaBH_4$	A_4	-1.63×10^0	kg/m^3 m_1^{-1} m_2^{-1}
$NaBH_4 \cdot NaOH$	A_5	-2.53×10^0	kg/m^3 m_2^{-1} m_3^{-1}
T	A_6	7.50×10^4	kg/m^3 K

[a]Densities are computed using MD simulations with the DFF/BH_4^-, the DFF/$B(OH)_4^-$,[56] Madrid-2019[58] Na^+ force field, DFF/OH^- force field,[55] and TIP4P/2005[62] water. These fitting parameters are for the concentration and temperature range of 0 to 5 m $NaBH_4$, 0 to 5 m $NaB(OH)_4$, 0 to 1 m NaOH, and 295–363 K. m^{-1} is in units of kg water/mol salt.

20%).[55,56,109−113] Based on these results, the DFF/BH_4^- force field, in combination with the other force fields [TIP4P/2005[62] water force field, Madrid-2019[58] Na^+ force field, DFF/OH^- force field[55] and DFF/$B(OH)_4^-$ force field[56], is considered to be sufficiently accurate for concentrations of 0 to 5 m $NaBH_4$, 0 to 5 m $NaB(OH)_4$ and 0 to 1 m NaOH and a temperature range from 295 to 363 K. Therefore, in the remainder of this work, we will focus on simulation results to formulate empirical correlations for densities, viscosities, and diffusion coefficients within the aforementioned concentration range.

Correlations for Salt Mixture Properties. For detailed reactor design purposes, a large data set of computed densities, viscosities, and self-diffusivities at different compositions of $NaBH_4$ and $NaB(OH)_4$ in aqueous solution is created at varying temperatures (323–363 K). All densities are computed from MD simulations for aqueous solutions of 1 to 5 m $NaBH_4$ and 0 to 5 m $NaB(OH)_4$ at different temperatures (323–363 K), as shown in Figure 5. It should be noted that the increase in the $NaBH_4$ concentration has an increasing and a decreasing effect on density depending on the absolute density value. This phenomenon is also found in experiments using a higher concentration of NaOH, as shown in Figure S3 of the Supporting Information. The following empirical correlation for the density has been created based on MD simulations data from different concentrations of 0 to 5 m $NaBH_4$, 0 to 5 m $NaB(OH)_4$, and 0 to 1 m NaOH in aqueous solutions at 295–363 K. The density at different temperatures is described using linear dependencies of concentrations and an inverse correlation for temperature, which is commonly used for density fitting of aqueous solutions.[114,115]

$$\rho = \rho_0 + A_1 m_1 + A_2 m_2 + A_3 m_3 + A_4 m_1 m_2 + A_5 m_2 m_3 + \frac{A_6}{T} \tag{8}$$

where m_1, m_2, and m_3 are the molalities (m) of $NaB(OH)_4$, $NaBH_4$, and NaOH, respectively, T is the absolute temperature, and ρ_0 and A_1...A_6 are the density fitting parameters. The cross terms A_4 and A_5 for the molalities of $NaB(OH)_4$ and $NaBH_4$ and $NaBH_4$ and NaOH are added to describe the influence of $NaBH_4$ on the density of the aqueous solution. The molality of $NaBH_4$ will decrease the density of the

https://doi.org/10.1021/acs.jced.4c00629
J. Chem. Eng. Data 2025, 70, 1830−1842

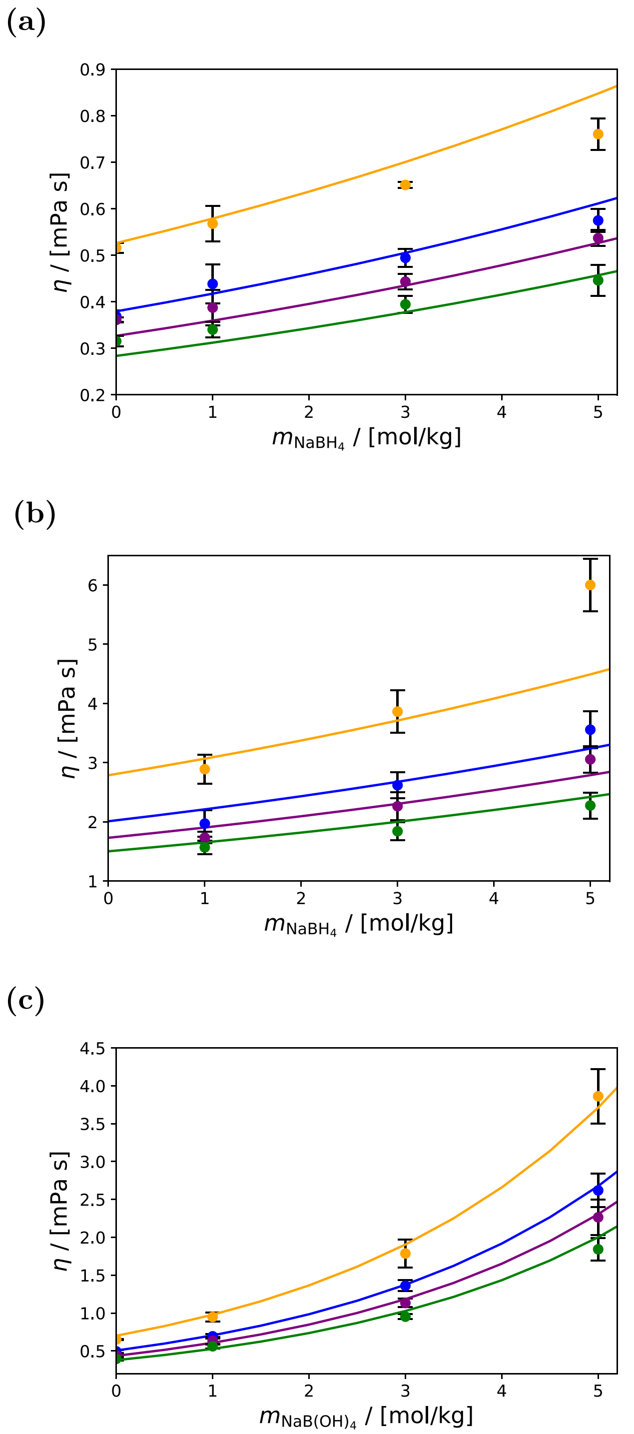

Figure 6. Computed viscosities (η) of $NaBH_4$ and $NaB(OH)_4$ aqueous solutions at 1 bar and 323 (yellow), 343 (blue), 353 (purple), and 363 (green) K are shown as circles in (a–c). (a) Viscosities for pure $NaBH_4$ aqueous solutions with the increasing $NaBH_4$ concentration at different temperatures. (b) Viscosities for $NaBH_4$ and $NaB(OH)_4$ aqueous solutions with a fixed $NaB(OH)_4$ concentration of 5 m and increasing $NaBH_4$ concentration at different temperatures. (c) Viscosities for $NaBH_4$ and $NaB(OH)_4$ aqueous solutions with a fixed $NaBH_4$ concentration of 3 m and increasing $NaB(OH)_4$ concentration at different temperatures. The empirical correlation is represented by solid lines and follows eq 9 with the parameters in Table 9. Uncertainties can be found in the Supporting Information Excel file provided.

Table 9. Viscosity (η) Fitting Parameters of Eq 9 for $NaBH_4$, $NaB(OH)_4$, and NaOH Aqueous Solutions[a]

dependency	parameter	value	
n.a.	η_0	1.93×10^{-3}	mPa s
$NaB(OH)_4$	B_1	3.34×10^{-1}	m_1^{-1}
$NaBH_4$	B_2	9.54×10^{-2}	m_2^{-1}
NaOH	B_3	2.49×10^{-1}	m_3^{-1}
T	B_4	1.81×10^{3}	K

[a]Viscosities are computed using MD simulations with the DFF/BH_4^-, the DFF/$B(OH)_4^-$,[56] Madrid-2019[58] Na^+ force field, DFF/OH^- force field,[55] and TIP4P/2005[62] water. These fitting parameters are for the concentration and temperature range of 0 to 5 m $NaBH_4$, 0 to 5 m $NaB(OH)_4$, 0 to 1 m NaOH, and 295–363 K. m^{-1} is in units of kg water/mol salt.

aqueous solution when the overall density is above a threshold (approximately 1000 kg/m^3). Similarly, the molality of $NaBH_4$ will increase the density of the aqueous solution when the overall density is below the threshold. This same behavior is also found in the density experiments with higher concentrations of NaOH, as shown in Figure S3 in the Supporting Information. It should be noted that for all empirical correlations, the simulations for pure water, NaOH aqueous solutions, $NaB(OH)_4$ solutions in water and $NaBH_4$ with NaOH aqueous mixtures at varying temperatures (295–363 K) are included in the correlation. The fitting parameters for the empirical density correlation are listed in Table 8. This empirical density correlation has an average deviation of 0.4% from the MD simulations.

All viscosities are computed from MD simulations for aqueous solutions of 1 to 5 m $NaBH_4$ and 0 to 5 m $NaB(OH)_4$ at different temperatures (323–363 K), as shown in Figure 6. The following empirical correlation for viscosity has been created based on MD simulations data from different concentrations of 0 to 5 m $NaBH_4$, 0 to 5 m $NaB(OH)_4$, and 0 to 1 m NaOH aqueous solutions at 295–363 K. The viscosity at different concentrations and temperatures is described using an exponential correlation for concentration and temperature, which is commonly used for fitting viscosities of aqueous solutions.[56,114,115]

$$\eta = \eta_0 \exp\left[B_1 m_1 + B_2 m_2 + B_3 m_3 + \frac{B_4}{T}\right] \tag{9}$$

where η_0 and $B_1 ... B_4$ are the viscosity fitting parameters. No cross terms are added to the empirical viscosity fit since no inconsistencies are found for the viscosity relation between $NaBH_4$, $NaB(OH)_4$ or NaOH molalities. The fitting parameters are listed in Table 9. The empirical correlation has an average deviation of 5.0% from the MD simulations.

All self-diffusivities of the BH_4^- are computed from MD simulations for aqueous solutions of 1 to 5 m $NaBH_4$ and 0 to 5 m $NaB(OH)_4$ at different temperatures (323–363 K), as shown in Figure 7. All values of self-diffusivity of BH_4^- are corrected for finite size effects using the Yeh–Hummer correction.[94,102–104] The following empirical correlation for self-diffusivity of BH_4^- (D_{self,BH_4^-}) has been created based on MD simulations data at different concentrations of 0.11 to 5 m $NaBH_4$, 0 to 5 m $NaB(OH)_4$, and 0 to 1 m NaOH aqueous solutions at 295–363 K. The self-diffusivity of BH_4^- at different concentrations and temperatures is described using an exponential correlation for concentration and temperature,

https://doi.org/10.1021/acs.jced.4c00629
J. Chem. Eng. Data 2025, 70, 1830–1842

(a)

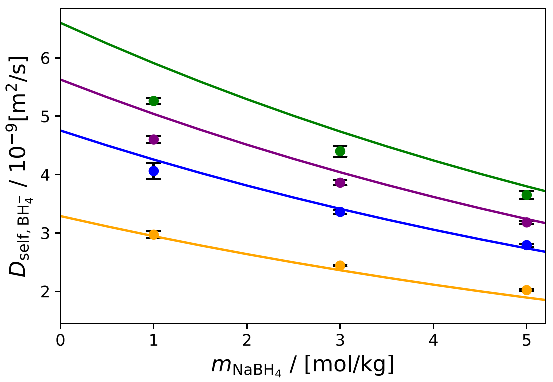

(b)

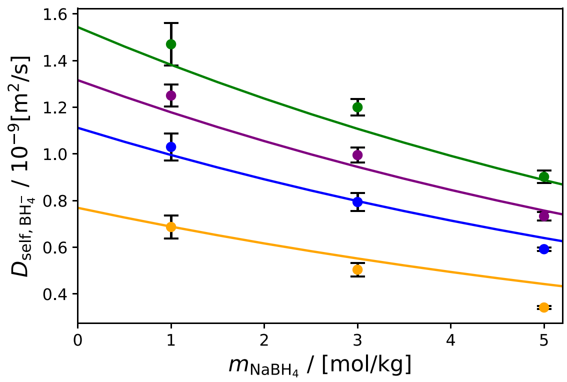

(c)

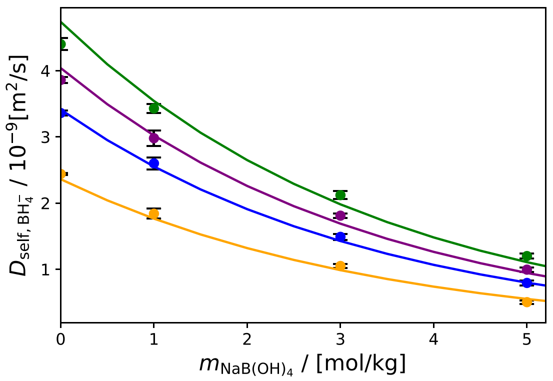

Figure 7. Computed self-diffusivities of BH_4^- (D_{self,BH_4^-}) for $NaBH_4$ and $NaB(OH)_4$ aqueous solutions at 1 bar and 323 (yellow), 343 (blue), 353 (purple), and 363 (green) K are shown as circles in (a–c). The self-diffusivities of BH_4^- are corrected for finite size effects using the Yeh–Hummer correction.[94,102−104] (a) Self-diffusivities of BH_4^- for pure $NaBH_4$ aqueous solutions with increasing $NaBH_4$ concentration at different temperatures. (b) Self-diffusivities of BH_4^- for $NaBH_4$ and $NaB(OH)_4$ aqueous solutions with a fixed $NaB(OH)_4$ concentration of 5 m and increasing $NaBH_4$ concentration at different temperatures. (c) Self-diffusivity of BH_4^- for $NaBH_4$ and $NaB(OH)_4$ aqueous solutions with a fixed $NaBH_4$ concentration of 3 m and increasing $NaB(OH)_4$ concentration at different temperatures. The empirical correlation is represented by solid lines and follows eq 10 with the parameters in Table 10. The error bars for self-diffusivity of BH_4^- are presented as one standard deviation. Uncertainties can be found in the Supporting Information Excel file provided.

Table 10. Self-Diffusivity of BH_4^- (D_{self,BH_4^-}) Fitting Parameters of Eq 10 for $NaBH_4$, $NaB(OH)_4$, and NaOH Aqueous Solutions[a]

dependency	parameter	value	
n.a.	$D_{self,0}$	1.83×10^{-6}	m^2/s
$NaB(OH)_4$	C_1	-2.91×10^{-1}	m_1^{-1}
$NaBH_4$	C_2	-1.11×10^{-1}	m_2^{-1}
NaOH	C_3	-2.07×10^{-1}	m_3^{-1}
T	C_4	-2.04×10^{3}	K

[a]Self-diffusivities of BH_4^- are computed using MD simulations with the DFF/BH_4^-, the DFF/$B(OH)_4^-$,[56] Madrid-2019[58] Na^+ force field, DFF/OH^- force field,[55] and TIP4P/2005[62] water. The self-diffusivities of BH_4^- are corrected for finite size effects using the Yeh–Hummer correction.[94,102−104] These fitting parameters are for the concentration and temperature range of 0 to 5 m $NaBH_4$, 0 to 5 m $NaB(OH)_4$, 0 to 1 m NaOH, and 295−363 K. m^{-1} is in units of kg water/mol salt.

which is commonly used for self-diffusivity fitting of aqueous solutions.[56,57]

$$D_{self,BH_4^-} = D_{self,0} \exp\left[C_1 m_1 + C_2 m_2 + C_3 m_3 + \frac{C_4}{T}\right] \tag{10}$$

where $D_{self,0}$ and $C_1 ... C_4$ are the self-diffusivity fitting parameters. Also here, no cross terms are added to the empirical self-diffusivity fit since no inconsistencies are found for the self-diffusion relation between $NaBH_4$, $NaB(OH)_4$ or NaOH molalities. The fitting parameters are listed in Table 10. The empirical correlation has an average deviation of 4.4% from the MD simulations.

■ CONCLUSIONS

The reactive nature of $NaBH_4$ in aqueous solution makes it difficult to experimentally determine thermodynamic and transport properties of aqueous $NaBH_4$ solutions, such as density and viscosity, especially at elevated temperatures. New experimental results for densities and viscosities are measured for 1−5 m $NaBH_4$ aqueous solutions, stabilized by 1 m of NaOH at 295 K. In this work, a new classical BH_4^- force field (DFF/BH_4^-) is developed (combined with the TIP4P/2005[62] water force field, Madrid-2019[58] Na^+ force field, and DFF/OH^- force field[55]) and optimized using the experimental results of stabilized $NaBH_4$ and NaOH aqueous solutions. The DFF/BH_4^- force field can accurately describe the densities and viscosities of $NaBH_4$ and NaOH aqueous solutions, in the concentration range of 0 to 5 m of $NaBH_4$ and 1 m of NaOH at 295 K and 1 bar, within 0.7% and 10.8% maximum deviation, respectively. The applicability of the DFF/BH_4^- force field is further tested with the addition of the DFF/$B(OH)_4^-$ force field[56] (in addition to the previously mentioned force fields) to the MD simulations. New experimental results for densities and viscosities are measured for 1−3 m $NaB(OH)_4$, 1 m $NaBH_4$, and 1 m NaOH stabilized aqueous solutions at 295 K. The combined force fields (TIP4P/2005[62] water force field, Madrid-2019[58] Na^+ force field, DFF/OH^- force field,[55] DFF/BH_4^- force field, and DFF/$B(OH)_4^-$ force field[56]) accurately describe the densities and viscosities of 0 to 3 m $NaB(OH)_4$, 1 m $NaBH_4$, and 1 m NaOH aqueous solutions at 295 K, within 1.8% and 8.3% maximum deviation, respectively. The MD simulations concentration and temperature range are extended to align with the expected application range of 0 to 5 m of $NaBH_4$ and 0 to 5 m of $NaB(OH)_4$ in

https://doi.org/10.1021/acs.jced.4c00629
J. Chem. Eng. Data 2025, 70, 1830−1842

aqueous solutions at 323−363 K. Empirical correlations have been derived for densities, viscosities, and self-diffusivities using only MD simulations results in the concentration range of 0 to 5 *m* $NaB(OH)_4$, 0 to 5 *m* $NaBH_4$, and 0 to 1 *m* NaOH and a temperature range of 295−363 K. The empirical correlations derived in this work provide the thermodynamic and transport properties needed for the modeling and design of $NaBH_4$ hydrolysis reactors at varying temperatures and salt compositions. The data used for these empirical correlations can be found in the Supporting Information Excel file. It should be noted that the force fields used in this work [TIP4P/2005[62] water force field, Madrid-2019[58] Na^+ force field, DFF/OH^- force field,[55] DFF/BH_4^- force field, and DFF/$B(OH)_4^-$ force field[56] are only optimized within their respected concentration and temperature ranges. The empirical correlation for densities overestimates the simulation data for pure aqueous solutions at low temperatures to a maximum deviation of 1.32% [0 *m* $NaBH_4$ and 0 *m* $NaB(OH)_4$ at 298 K]. The empirical correlation for viscosities underestimates the simulation data at higher combined concentrations of $NaBH_4$ and $NaB(OH)_4$ at lower temperatures to a maximum deviation of 25.2% [5 *m* $NaBH_4$ and 5 *m* $NaB(OH)_4$ at 323 K]. The empirical correlation for self-diffusivities of BH_4^- overestimates the simulation data at higher combined concentrations of $NaBH_4$ and $NaB(OH)_4$ at lower temperatures to a maximum deviation of 29.5% [5 *m* $NaBH_4$ and 5 *m* $NaB(OH)_4$ at 323 K]. It is not advised to use empirical correlations outside the recommended concentration and temperature range. It should be noted that $NaB(OH)_4$ has a higher influence on both densities and viscosities than $NaBH_4$, which makes the empirical correlation more suited for high concentrations of $NaB(OH)_4$ (more than 5 *m*) with lower concentrations of $NaBH_4$ (0 to 3 *m*) as shown in Figure S2 of the Supporting Information. It should also be noted that the DFF/$B(OH)_4^-$ force field[56] is not optimized for higher concentrations of $NaB(OH)_4$ (more than 5 *m*). We recommend, for future research, expanding the DFF/BH_4^- force field to cations such as K^+ for applications of KBH_4 as another potential hydrogen carrier.

■ ASSOCIATED CONTENT

Supporting Information

The Supporting Information is available free of charge at https://pubs.acs.org/doi/10.1021/acs.jced.4c00629.

Force field parameters; viscosity measurements; computed MD simulations of viscosity for elevated (1−11 *m*) molalities (mol salt/kg water) of $NaB(OH)_4$ with 1 *m* $NaBH_4$ and 1 *m* NaOH at 353 K and 1 bar; computed densities and viscosities for the elevated molalities of $NaB(OH)_4$ with 1 *m* $NaBH_4$ and 1 *m* NaOH at 353 K and 1 bar; experimental densities (ρ) for different concentrations of NaOH, and $NaBH_4$ concentration in aqueous solution; experimental densities (ρ) and one standard deviation of the experimental densities (ρ_{error}) for different concentrations of $NaBH_4$ and NaOH in aqueous solution; $MSD_{D_{i,self}}$ equation used for Figure S5 (eq S1); $MSD_{D_{i,self}}$ equation used for Figure S5 (eq S2); RDFs $g(r)$ versus radial distance [Å] for different ion and atom combinations with Na^+ mean square displacement curves for calculating self-diffusivity and shear viscosity; and MD densities and one standard deviation for optimization of the DFF/BH_4^- (PDF)

Sample simulation files for the MD simulations in LAMMPS software (ZIP)

All MD simulation data used for development of the empirical correlations of density, viscosity, and self-diffusivity (BH_4^-) (corrected with Yeh−Hummer); all self-diffusivities of Na^+ and H_2O and the self-diffusivities of Na^+, BH_4^- and H_2O which are not corrected for finite size effects (no Yeh−Hummer corrections); and uncertainties of densities (ρ_{error}), viscosities (η_{error}) and self-diffusivities $D_{i,error}$ (Na^+, BH_4^- and H_2O) for all MD simulations (XLSX)

■ AUTHOR INFORMATION

Corresponding Author

Johan T. Padding − *Complex Fluid Processing, Process & Energy Department, Faculty of Mechanical Engineering, Delft University of Technology, 2628 CB Delft, The Netherlands;* orcid.org/0000-0003-4161-0748; Email: J.T.Padding@tudelft.nl

Authors

Julien R. T. Postma − *Complex Fluid Processing, Process & Energy Department, Faculty of Mechanical Engineering, Delft University of Technology, 2628 CB Delft, The Netherlands*

Parsa Habibi − *Engineering Thermodynamics, Process & Energy Department, Faculty of Mechanical Engineering, Delft University of Technology, 2628 CB Delft, The Netherlands; Department of Materials Science and Engineering, Faculty of Mechanical Engineering, Delft University of Technology, 2628 CD Delft, The Netherlands*

Poulumi Dey − *Department of Materials Science and Engineering, Faculty of Mechanical Engineering, Delft University of Technology, 2628 CD Delft, The Netherlands;* orcid.org/0000-0003-4679-1752

Thijs J. H. Vlugt − *Engineering Thermodynamics, Process & Energy Department, Faculty of Mechanical Engineering, Delft University of Technology, 2628 CB Delft, The Netherlands;* orcid.org/0000-0003-3059-8712

Othonas A. Moultos − *Engineering Thermodynamics, Process & Energy Department, Faculty of Mechanical Engineering, Delft University of Technology, 2628 CB Delft, The Netherlands;* orcid.org/0000-0001-7477-9684

Complete contact information is available at: https://pubs.acs.org/10.1021/acs.jced.4c00629

Notes

The authors declare no competing financial interest.

■ ACKNOWLEDGMENTS

This work was supported by the project SH2IPDRIVE: Sustainable Hydrogen Integrated Propulsion Drives, funded by the RvO (reference number MOB21013), through the RDM regulations of Ministry of Economic Affairs and Climate Policy. This work was sponsored by NWO Domain Science for the use of supercomputer facilities. The authors acknowledge the use of computational resources of the DelftBlue supercomputer, provided by Delft High Performance Computing Centre (https://www.tudelft.nl/dhpc).

■ REFERENCES

(1) Stančin, H.; Mikulčić, H.; Wang, X.; Duić, N. A review on alternative fuels in future energy system. *Renew. Sustain. Energy Rev.* **2020**, *128*, 109927.

(2) Prasad, S.; Singh, A.; Joshi, H. C. Ethanol as an alternative fuel from agricultural, industrial and urban residues. *Resour. Conserv. Recycl.* **2007**, *50*, 1−39.

(3) Sangeeta; Moka, S.; Pande, M.; Rani, M.; Gakhar, R.; Sharma, M.; Rani, J.; Bhaskarwar, A. N. Alternative fuels: An overview of current trends and scope for future. *Renew. Sustain. Energy Rev.* **2014**, *32*, 697−712.

(4) Ramadhas, A. S. *Alternative Fuels for Transportation*; CRC Press, 2011.

(5) Bouman, E. A.; Lindstad, E.; Rialland, A. I.; Strømman, A. H. State-of-the-art technologies, measures, and potential for reducing GHG emissions from shipping − A review. *Transp. Res. D Trans. Environ.* **2017**, *52*, 408−421.

(6) Barreto, R. A. Fossil fuels, alternative energy and economic growth. *Econ. Modell.* **2018**, *75*, 196−220.

(7) Ramesohl, S.; Merten, F. Energy system aspects of hydrogen as an alternative fuel in transport. *Energy Policy* **2006**, *34*, 1251−1259.

(8) van Rheenen, E.; Padding, J.; Slootweg, C.; Visser, K. A review of the potential of hydrogen carriers for zero emission, low signature ship propulsion systems. 2021, http://library.imarest.org/record/10649 (accessed June 30, 2023).

(9) Dragan, M. Hydrogen Storage in Complex Metal Hydrides $NaBH_4$: Hydrolysis Reaction and Experimental Strategies. *Catalysts* **2022**, *12*, 356.

(10) Qazi, U. Y. Future of Hydrogen as an Alternative Fuel for Next-Generation Industrial Applications; Challenges and Expected Opportunities. *Energies* **2022**, *15*, 4741.

(11) Atilhan, S.; Park, S.; El-Halwagi, M. M.; Atilhan, M.; Moore, M.; Nielsen, R. B. Green hydrogen as an alternative fuel for the shipping industry. *Curr. Opin. Chem. Eng.* **2021**, *31*, 100668.

(12) da Silva Veras, T.; Mozer, T. S.; da Costa Rubim Messeder dos Santos, D.; da Silva César, A. Hydrogen: Trends, production and characterization of the main process worldwide. *Int. J. Hydrogen Energy* **2017**, *42*, 2018−2033.

(13) Abdelhamid, H. N. A review on hydrogen generation from the hydrolysis of sodium borohydride. *Int. J. Hydrogen Energy* **2021**, *46*, 726−765.

(14) Marrero-Alfonso, E. Y.; Beaird, A. M.; Davis, T. A.; Matthews, M. A. Hydrogen generation from chemical hydrides. *Ind. Eng. Chem. Res.* **2009**, *48*, 3703−3712.

(15) Hwang, H. T.; Varma, A. Hydrogen storage for fuel cell vehicles. *Curr. Opin. Chem. Eng.* **2014**, *5*, 42−48.

(16) Sinigaglia, T.; Lewiski, F.; Santos Martins, M. E.; Mairesse Siluk, J. C. Production, storage, fuel stations of hydrogen and its utilization in automotive applications-a review. *Int. J. Hydrogen Energy* **2017**, *42*, 24597−24611.

(17) Al-Zohbi, G.; Almoaikel, A.; Al-Shuhail, L. An overview on the technologies used to store hydrogen. *Energy Rep.* **2023**, *9*, 28−34.

(18) Zou, Y. C.; Nie, M.; Huang, Y. M.; Wang, J. Q.; Liu, H. L. Kinetics of $NaBH_4$ hydrolysis on carbon-supported ruthenium catalysts. *Int. J. Hydrogen Energy* **2011**, *36*, 12343−12351.

(19) Retnamma, R.; Novais, A. Q.; Rangel, C. M.; Yu, L.; Matthews, M. A. Kinetic modeling of self-hydrolysis of aqueous $NaBH_4$ solutions by model-based isoconversional method. *Int. J. Hydrogen Energy* **2014**, *39*, 6567−6576.

(20) Mosier-Boss, P. A.; Becker, C. A.; Anderson, G. W.; Wiedemeier, B. J. Feasibility Studies of the $NaBH_4/H_2O$ Hydrolysis to Generate Hydrogen Gas to Inflate Lighter than Air (LTA) Vehicles. *Ind. Eng. Chem. Res.* **2015**, *54*, 7706−7714.

(21) Rusman, N. A.; Dahari, M. A review on the current progress of metal hydrides material for solid-state hydrogen storage applications. *Int. J. Hydrogen Energy* **2016**, *41*, 12108−12126.

(22) Zhang, Q.; Mohring, R. M. Reaction chemistry between aqueous sulfuric acid and solid sodium borohydride. *Ind. Eng. Chem. Res.* **2009**, *48*, 1603−1607.

(23) Hojjati-Najafabadi, A.; Aygun, A.; Tiri, R. N. E.; Gulbagca, F.; Lounissaa, M. I.; Feng, P.; Karimi, F.; Sen, F. Bacillus thuringiensis Based Ruthenium/Nickel Co-Doped Zinc as a Green Nanocatalyst: Enhanced Photocatalytic Activity, Mechanism, and Efficient H_2 Production from Sodium Borohydride Methanolysis. *Ind. Eng. Chem. Res.* **2023**, *62*, 4655−4664.

(24) Andrieux, J.; Demirci, U. B.; Hannauer, J.; Gervais, C.; Goutaudier, C.; Miele, P. Spontaneous hydrolysis of sodium borohydride in harsh conditions. *Int. J. Hydrogen Energy* **2011**, *36*, 224−233.

(25) Gonçalves, A.; Castro, P.; Novais, A. Q.; Rangel, C. M.; Matos, H. Modeling of catalytic hydrogen generation from sodium borohydride. *Comput.-Aided Chem. Eng.* **2008**, *25*, 757−762.

(26) Stepanov, N.; Uvarov, V.; Popov, I.; Sasson, Y. Study of by-product of $NaBH_4$ hydrolysis and its behavior at a room temperature. *Int. J. Hydrogen Energy* **2008**, *33*, 7378−7384.

(27) Ye, W.; Zhang, H.; Xu, D.; Ma, L.; Yi, B. Hydrogen generation utilizing alkaline sodium borohydride solution and supported cobalt catalyst. *J. Power Sources* **2007**, *164*, 544−548.

(28) Wang, Y.; Hu, Z.; Chen, W.; Wu, S.; Li, G.; Chou, S. Non-Noble Metal-Based Catalysts Applied to Hydrogen Evolution from Hydrolysis of Boron Hydrides. *Small Struct.* **2021**, *2*, 2000135.

(29) Brack, P.; Dann, S. E.; Wijayantha, K. G. U. Heterogeneous and homogenous catalysts for hydrogen generation by hydrolysis of aqueous sodium borohydride ($NaBH_4$) solutions. *Energy Sci. Eng.* **2015**, *3*, 174−188.

(30) Li, Y.; Zhang, X.; Zhang, Q.; Zheng, J. B.; Zhang, N.; Chen, B. H.; Smith, K. J. Activity and kinetics of ruthenium supported catalysts for sodium borohydride hydrolysis to hydrogen. *RSC Adv.* **2016**, *6*, 29371−29377.

(31) Demirci, U. B.; Akdim, O.; Andrieux, J.; Hannauer, J.; Chamoun, R.; Miele, P. Sodium borohydride hydrolysis as hydrogen generator: issues, state of the art and applicability upstream from a fuel cell. *Fuel Cells* **2010**, *10*, 335−350.

(32) Kim, K.; Kim, T.; Lee, K.; Kwon, S. Fuel cell system with sodium borohydride as hydrogen source for unmanned aerial vehicles. *J. Power Sources* **2011**, *196*, 9069−9075.

(33) Nunes, H. X.; Ferreira, M. J.; Rangel, C. M.; Pinto, A. M. Hydrogen generation and storage by aqueous sodium borohydride ($NaBH_4$) hydrolysis for small portable fuel cells (H_2 − PEMFC). *Int. J. Hydrogen Energy* **2016**, *41*, 15426−15432.

(34) Sakamoto, Y.; Hoshi, N.; Murooka, S.; Cao, M.; Yoshizaki, A.; Hirata, K. Basic study on fuel-cell-hybrid-electric-vehicle fueled by sodium borohydride. In *The 2010 International Power Electronics Conference—ECCE ASIA*, 2010; pp 814−819.

(35) Santos, D. M. F.; Sequeira, C. A. Sodium borohydride as a fuel for the future. *Renew. Sustain. Energy Rev.* **2011**, *15*, 3980−4001.

(36) Kaya, C. Sodium Borohydride ($NaBH_4$) as a Maritime Transportation Fuel. *Hydrogen* **2024**, *5*, 540−558.

(37) Malaeb, L.; Ayoub, G. M. Reverse osmosis technology for water treatment: State of the art review. *Desalination* **2011**, *267*, 1−8.

(38) Peters, C. D.; Hankins, N. P. Osmotically assisted reverse osmosis (OARO): Five approaches to dewatering saline brines using pressure-driven membrane processes. *Desalination* **2019**, *458*, 1−13.

(39) Lensing, D. A study on the integration of a novel $NaBH_4$ fueled hybrid system for a small inland vessel. Master Thesis, 2020.

(40) van Nievelt, F. Maritime application of sodium borohydride as an energy carrier. Ph.D. Thesis, 2019.

(41) Zhang, J. S.; Delgass, W. N.; Fisher, T. S.; Gore, J. P. Kinetics of Ru-catalyzed sodium borohydride hydrolysis. *J. Power Sources* **2007**, *164*, 772−781.

(42) Churikov, A. V.; Gamayunova, I. M.; Zapsis, K. V.; Churikov, M. A.; Ivanishchev, A. V. Influence of temperature and alkalinity on the hydrolysis rate of borohydride ions in aqueous solution. *Int. J. Hydrogen Energy* **2012**, *37*, 335−344.

(43) Moon, G. Y.; Lee, S. S.; Lee, K. Y.; Kim, S. H.; Song, K. H. Behavior of hydrogen evolution of aqueous sodium borohydride solutions. *J. Ind. Eng. Chem.* **2008**, *14*, 94−99.

https://doi.org/10.1021/acs.jced.4c00629
J. Chem. Eng. Data 2025, 70, 1830−1842

(44) Bartkus, T. P.; T'Ien, J. S.; Sung, C. J. A semi-global reaction rate model based on experimental data for the self-hydrolysis kinetics of aqueous sodium borohydride. *Int. J. Hydrogen Energy* **2013**, *38*, 4024−4033.

(45) Minkina, V. G.; Shabunya, S. I.; Kalinin, V. I.; Martynenko, V. V.; Smirnova, A. L. Stability of alkaline aqueous solutions of sodium borohydride. *Int. J. Hydrogen Energy* **2012**, *37*, 3313−3318.

(46) Zhang, Q.; Wu, Y.; Sun, X.; Ortega, J. Kinetics of catalytic hydrolysis of stabilized sodium borohydride solutions. *Ind. Eng. Chem. Res.* **2007**, *46*, 1120−1124.

(47) Wang, Q.; Zhang, L. F.; Zhao, Z. G. Hydrogen production by sodium borohydride in NaOH aqueous solution. *IOP Conf. Ser. Mater. Sci. Eng.* **2018**, *292*, 012031.

(48) Kojima, Y.; Suzuki, K. I.; Fukumoto, K.; Kawai, Y.; Kimbara, M.; Nakanishi, H.; Matsumoto, S. Development of 10 kW-scale hydrogen generator using chemical hydride. *J. Power Sources* **2004**, *125*, 22−26.

(49) Sousa, T.; Fernandes, V. R.; Pinto, P. J.; Slavkov, Y.; Bosukov, L.; Rangel, C. M. A sodium borohydride hydrogen generation reactor for stationary applications: Experimental and reactor simulation studies. *Chem. Eng. Sci.* **2012**, *84*, 70−79.

(50) Zhang, J.; Zheng, Y.; Gore, J. P.; Fisher, T. S. 1 kWe sodium borohydride hydrogen generation system. Part I: Experimental study. *J. Power Sources* **2007**, *165*, 844−853.

(51) Zhang, J.; Zheng, Y.; Gore, J. P.; Mudawar, I.; Fisher, T. S. 1 kWe sodium borohydride hydrogen generation system. Part II: Reactor modeling. *J. Power Sources* **2007**, *170*, 150−159.

(52) Zaykovskaya, A.; Louhi-Kultanen, M. Cooling and Evaporative Crystallization of α-D-Galactose from a Highly Viscous Industrial Side Stream. *Chem. Eng. Technol.* **2023**, *46*, 2330−2336.

(53) Zaykovskaya, A.; Louhi-Kultanen, M. Batch Crystallization of Xylitol by Cooling, Evaporative, and Antisolvent Crystallization. *Cryst. Growth Des.* **2023**, *23*, 1813−1820.

(54) Kaya, M.; Ceyhan, A. A.; Şahin, O. Effects of different temperatures and additives on the metastable zone width precipitation kinetics of $NaBO_2$. *Russ. J. Phys. Chem. A* **2014**, *88*, 402−408.

(55) Habibi, P.; Rahbari, A.; Blazquez, S.; Vega, C.; Dey, P.; Vlugt, T. J.; Moultos, O. A. A New Force Field for OH^- for Computing Thermodynamic and Transport Properties of H_2 and O_2 in Aqueous NaOH and KOH Solutions. *J. Phys. Chem. B* **2022**, *126*, 9376−9387.

(56) Habibi, P.; Postma, J. R. T.; Padding, J. T.; Dey, P.; Vlugt, T. J. H.; Moultos, O. A. Thermodynamic and Transport Properties of H_2/H_2O/$NaB(OH)_4$ Mixtures Using the Delft Force Field (DFF/$B(OH)_4^-$). *Ind. Eng. Chem. Res.* **2023**, *62*, 11992−12005.

(57) van Rooijen, W. A.; Habibi, P.; Xu, K.; Dey, P.; Vlugt, T. J.; Hajibeygi, H.; Moultos, O. A. Interfacial Tensions, Solubilities, and Transport Properties of the H_2/H_2O/NaCl System: A Molecular Simulation Study. *J. Chem. Eng. Data* **2024**, *69*, 307−319.

(58) Zeron, I. M.; Abascal, J. L. F.; Vega, C. A force field of Li^+, Na^+, K^+, Mg^{2+}, Ca^{2+}, Cl^-, and SO_4^{2-}in aqueous solution based on the TIP4P/2005 water model and scaled charges for the ions. *J. Chem. Phys.* **2019**, *151*, 134504.

(59) Núñez-Rojas, E.; González, I.; Guzmán-González, G.; Alejandre, J. Molecular dynamics simulations for liquid electrolytes of propylene carbonate with LiTFSI, LiPF6, and LiBF4 salts. *J. Mol. Liq.* **2023**, *390*, 122983.

(60) Li, P. Phase Behavior and Reaction Mechanism Study of Hydrogen Storage in Sodium Borohydride. Ph.D. Thesis, 2013.

(61) Ewoldt, R. H.; Johnston, M. T.; Caretta, L. M. In *Complex Fluids in Biological Systems: Experiment, Theory, and Computation*; Spagnolie, S. E., Ed.; Springer New York: New York, NY, 2015; pp 207−241.

(62) Abascal, J. L. F.; Vega, C. A general purpose model for the condensed phases of water: TIP4P/2005. *J. Chem. Phys.* **2005**, *123*, 234505.

(63) Tsimpanogiannis, I. N.; Maity, S.; Celebi, A. T.; Moultos, O. A. Engineering Model for Predicting the Intradiffusion Coefficients of Hydrogen and Oxygen in Vapor, Liquid, and Supercritical Water based on Molecular Dynamics Simulations. *J. Chem. Eng. Data* **2021**, *66*, 3226−3244.

(64) Vega, C.; Abascal, J. L. F. Simulating water with rigid non-polarizable models: a general perspective. *Phys. Chem. Chem. Phys.* **2011**, *13*, 19663−19688.

(65) Vega, C.; de Miguel, E. Surface tension of the most popular models of water by using the test-area simulation method. *J. Chem. Phys.* **2007**, *126*, 154707.

(66) Tsimpanogiannis, I. N.; Moultos, O. A.; Franco, L. F. M.; Spera, M. B. d. M.; Erdős, M.; Economou, I. G. Self-diffusion coefficient of bulk and confined water: a critical review of classical molecular simulation studies. *Mol. Simul.* **2019**, *45*, 425−453.

(67) Moultos, O. A.; Tsimpanogiannis, I. N.; Panagiotopoulos, A. Z.; Economou, I. G. Atomistic molecular dynamics simulations of CO_2 diffusivity in H_2O for a wide range of temperatures and pressures. *J. Phys. Chem. B* **2014**, *118*, 5532−5541.

(68) Döpke, M. F.; Moultos, O. A.; Hartkamp, R. On the transferability of ion parameters to the TIP4P/2005 water model using molecular dynamics simulations. *J. Chem. Phys.* **2020**, *152*, 024501.

(69) Leontyev, I. V.; Stuchebrukhov, A. A. Electronic Polarizability and the Effective Pair Potentials of Water. *J. Chem. Theory Comput.* **2010**, *6*, 3153−3161.

(70) Lee, D. Y.; Li, Y. Y.; Noike, T. Continuous H_2 production by anaerobic mixed microflora in membrane bioreactor. *Bioresour. Technol.* **2009**, *100*, 690−695.

(71) Leontyev, I.; Stuchebrukhov, A. Accounting for electronic polarization in non-polarizable force fields. *Phys. Chem. Chem. Phys.* **2011**, *13*, 2613−2626.

(72) Li, P.; Henkelman, G.; Keith, J. A.; Johnson, J. K. Elucidation of aqueous solvent-mediated hydrogen-transfer reactions by ab initio molecular dynamics and nudged elastic-band studies of $NaBH_4$ hydrolysis. *J. Phys. Chem. C* **2014**, *118*, 21385−21399.

(73) Leontyev, I. V.; Stuchebrukhov, A. A. Polarizable mean-field model of water for biological simulations with AMBER and CHARMM force fields. *J. Chem. Theory Comput.* **2012**, *8*, 3207−3216.

(74) Leontyev, I. V.; Stuchebrukhov, A. A. Polarizable molecular interactions in condensed phase and their equivalent nonpolarizable models. *J. Chem. Phys.* **2014**, *141*, 014103.

(75) Martin, M. G.; Siepmann, J. I. Transferable Potentials for Phase Equilibria. 1. United-Atom Description of n-Alkanes. *J. Phys. Chem. B* **1998**, *102*, 2569−2577.

(76) Frenkel, D.; Smit, B. In *Understanding Molecular Simulation*, 3rd ed.; Frenkel, D., Smit, B., Eds.; Academic Press, 2023.

(77) Allen, M.; Tildesley, D. *Computer Simulation of Liquids*, 2nd ed.; Oxford Science Publications: Oxford University Press: New York, 2017.

(78) Plimpton, S. Fast Parallel Algorithms for Short-Range Molecular Dynamics. *J. Comput. Phys.* **1995**, *117*, 1−19.

(79) Ryckaert, J. P.; Ciccotti, G.; Berendsen, H. J. Numerical integration of the cartesian equations of motion of a system with constraints: molecular dynamics of n-alkanes. *J. Comput. Phys.* **1977**, *23*, 327−341.

(80) Nguyen, T. D.; Phillips, C. L.; Anderson, J. A.; Glotzer, S. C. Rigid body constraints realized in massively-parallel molecular dynamics on graphics processing units. *Comput. Phys. Commun.* **2011**, *182*, 2307−2313.

(81) Hockney, W. R.; Eastwood, J. W. *Computer Simulation Using Particles*, 1st ed.; CRC Press: Boca Raton, 1988.

(82) Luty, B. A.; Davis, M. E.; Tironi, I. G.; Van Gunsteren, W. F. A Comparison of Particle-Particle, Particle-Mesh and Ewald Methods for Calculating Electrostatic Interactions in Periodic Molecular Systems. *Mol. Simul.* **1994**, *14*, 11−20.

(83) Pollock, E. L.; Glosli, J. Comments on P3M, FMM, and the Ewald method for large periodic Coulombic systems. *Comput. Phys. Commun.* **1996**, *95*, 93−110.

(84) Verlet, L. Computer "Experiments" on Classical Fluids. I. Thermodynamical Properties of Lennard-Jones Molecules. *Phys. Rev.* **1967**, *159*, 98−103.

https://doi.org/10.1021/acs.jced.4c00629
J. Chem. Eng. Data 2025, 70, 1830−1842

(85) Nosé, S. A unified formulation of the constant temperature molecular dynamics methods. *J. Chem. Phys.* **1984**, *81*, 511−519.
(86) Hoover, W. G. Canonical dynamics: Equilibrium phase-space distributions. *Phys. Rev. A: At., Mol., Opt. Phys.* **1985**, *31*, 1695−1697.
(87) Kamberaj, H.; Low, R. J.; Neal, M. P. Time reversible and symplectic integrators for molecular dynamics simulations of rigid molecules. *J. Chem. Phys.* **2005**, *122*, 224114.
(88) Jamali, S. H.; Wolff, L.; Becker, T. M.; De Groen, M.; Ramdin, M.; Hartkamp, R.; Bardow, A.; Vlugt, T. J.; Moultos, O. A. OCTP: A Tool for On-the-Fly Calculation of Transport Properties of Fluids with the Order- n Algorithm in LAMMPS. *J. Chem. Inf. Model.* **2019**, *59*, 1290−1294.
(89) Martínez, L.; Andrade, R.; Birgin, E. G.; Martínez, J. M. PACKMOL: A package for building initial configurations for molecular dynamics simulations. *J. Comput. Chem.* **2009**, *30*, 2157−2164.
(90) Mondello, M.; Grest, G. S. Viscosity calculations of n-alkanes by equilibrium molecular dynamics. *J. Chem. Phys.* **1997**, *106*, 9327−9336.
(91) Tenney, C.; Maginn, E. Limitations and recommendations for the calculation of shear viscosity using reverse nonequilibrium molecular dynamics. *J. Chem. Phys.* **2010**, *132*, 014103.
(92) Zwanzig, R. Time-Correlation Functions and Transport Coefficients in Statistical Mechanics. *Annu. Rev. Phys. Chem.* **1965**, *16*, 67−102.
(93) Jamali, S. H.; Wolff, L.; Becker, T. M.; Bardow, A.; Vlugt, T. J.; Moultos, O. A. Finite-Size Effects of Binary Mutual Diffusion Coefficients from Molecular Dynamics. *J. Chem. Theory Comput.* **2018**, *14*, 2667−2677.
(94) Celebi, A. T.; Jamali, S. H.; Bardow, A.; Vlugt, T. J. H.; Moultos, O. A. Finite-size effects of diffusion coefficients computed from molecular dynamics: a review of what we have learned so far. *Mol. Simul.* **2021**, *47*, 831−845.
(95) Jamali, S. H.; Hartkamp, R.; Bardas, C.; Söhl, J.; Vlugt, T. J.; Moultos, O. A. Shear Viscosity Computed from the Finite-Size Effects of Self-Diffusivity in Equilibrium Molecular Dynamics. *J. Chem. Theory Comput.* **2018**, *14*, 5959−5968.
(96) Moultos, O. A.; Zhang, Y.; Tsimpanogiannis, I. N.; Economou, I. G.; Maginn, E. J. System-size corrections for self-diffusion coefficients calculated from molecular dynamics simulations: The case of CO_2, n-alkanes, and poly(ethylene glycol) dimethyl ethers. *J. Chem. Phys.* **2016**, *145*, 074109.
(97) Krishna, R.; Van Baten, J. M. The Darken relation for multicomponent diffusion in liquid mixtures of linear alkanes: An investigation using Molecular Dynamics (MD) simulations. *Ind. Eng. Chem. Res.* **2005**, *44*, 6939−6947.
(98) Liu, X.; Schnell, S. K.; Simon, J.-M.; Krüger, P.; Bedeaux, D.; Kjelstrup, S.; Bardow, A.; Vlugt, T. J. H. Diffusion Coefficients from Molecular Dynamics Simulations in Binary and Ternary Mixtures. *Int. J. Thermophys.* **2013**, *34*, 1169−1196.
(99) Liu, X.; Schnell, S. K.; Simon, J. M.; Bedeaux, D.; Kjelstrup, S.; Bardow, A.; Vlugt, T. J. Fick diffusion coefficients of liquid mixtures directly obtained from equilibrium molecular dynamics. *J. Phys. Chem. B* **2011**, *115*, 12921−12929.
(100) Liu, X.; Vlugt, T. J.; Bardow, A. Maxwell-stefan diffusivities in binary mixtures of ionic liquids with dimethyl sulfoxide (DMSO) and H_2O. *J. Phys. Chem. B* **2011**, *115*, 8506−8517.
(101) Liu, X.; Vlugt, T. J.; Bardow, A. Maxwell−Stefan diffusivities in liquid mixtures: Using molecular dynamics for testing model predictions. *Fluid Phase Equilib.* **2011**, *301*, 110−117.
(102) Yeh, I.-C.; Hummer, G. System-size dependence of diffusion coefficients and viscosities from molecular dynamics simulations with periodic boundary conditions. *J. Phys. Chem. B* **2004**, *108*, 15873−15879.
(103) Dünweg, B.; Kremer, K. Molecular dynamics simulation of a polymer chain in solution. *J. Chem. Phys.* **1993**, *99*, 6983−6997.
(104) Jamali, S. H.; Bardow, A.; Vlugt, T. J.; Moultos, O. A. Generalized Form for Finite-Size Corrections in Mutual Diffusion Coefficients of Multicomponent Mixtures Obtained from Equilibrium Molecular Dynamics Simulation. *J. Chem. Theory Comput.* **2020**, *16*, 3799−3806.
(105) Delft High Performance Computing Centre (DHPC), DelftBlue Supercomputer (Phase 1). 2022, https://www.tudelft.nl/dhpc/ark:/44463/DelftBluePhase1 (accessed June 30, 2023).
(106) Richardson, B. S.; Birdwell, J. F.; Pin, F. G.; Jansen, J. F.; Lind, R. F. Sodium borohydride based hybrid power system. *J. Power Sources* **2005**, *145*, 21−29.
(107) Joung, I. S.; Cheatham, T. E. Determination of alkali and halide monovalent ion parameters for use in explicitly solvated biomolecular simulations. *J. Phys. Chem. B* **2008**, *112*, 9020−9041.
(108) Wang, K.; Lu, J.; Zhuang, L. Direct determination of diffusion coefficient for borohydride anions in alkaline solutions using chronoamperometry with spherical Au electrodes. *J. Electroanal. Chem.* **2005**, *585*, 191−196.
(109) Celebi, A. T.; Vlugt, T. J.; Moultos, O. A. Structural, Thermodynamic, and Transport Properties of Aqueous Reline and Ethaline Solutions from Molecular Dynamics Simulations. *J. Phys. Chem. B* **2019**, *123*, 11014−11025.
(110) Galliéro, G.; Boned, C.; Baylaucq, A. Molecular dynamics study of the Lennard-Jones fluid viscosity: Application to real fluids. *Ind. Eng. Chem. Res.* **2005**, *44*, 6963−6972.
(111) Yang, X.; Liu, Q.; Zhang, X.; Ji, C.; Cao, B. A molecular dynamics simulation study of the densities and viscosities of 1,2,4-trimethylbenzene and its binary mixture with n-decane. *Fluid Phase Equilib.* **2022**, *562*, 113566.
(112) Saric, D.; Kohns, M.; Vrabec, J. Dielectric constant and density of aqueous alkali halide solutions by molecular dynamics: A force field assessment. *J. Chem. Phys.* **2020**, *152*, 164502.
(113) Guevara-Carrion, G.; Nieto-Draghi, C.; Vrabec, J.; Hasse, H. Prediction of transport properties by molecular simulation: Methanol and their mixture. *J. Phys. Chem. B* **2008**, *112*, 16664−16674.
(114) Zhang, J.; Fennell, P. S.; Trusler, J. P. M. Density and Viscosity of Partially Carbonated Aqueous Tertiary Alkanolamine Solutions at Temperatures between (298.15 and 353.15) K. *J. Chem. Eng. Data* **2015**, *60*, 2392−2399.
(115) Patzschke, C. F.; Zhang, J.; Fennell, P. S.; Trusler, J. P. M. Density and Viscosity of Partially Carbonated Aqueous Solutions Containing a Tertiary Alkanolamine and Piperazine at Temperatures between 298.15 and 353.15 K. *J. Chem. Eng. Data* **2017**, *62*, 2075−2083.

https://doi.org/10.1021/acs.jced.4c00629
J. Chem. Eng. Data 2025, 70, 1830−1842